Integrating simulation and measurement techniques to model outdoor noise and heat in airport neighbourhoods with varying urban geometries

Wuite, Gustaf; Peng, Zhikai; Kim, Kyujin; Lugten, Martijn; Tenpierik, Martin

DOI
10.26868/25222708.2023.1388

Publication date
2024

Document Version
Final published version

Published in
Proceedings of Building Simulation 2023

BS 2023 4-6 SEPT SHANGHAI

International Building Performance Simulation Association

Integrating Simulation and Measurement Techniques to Model Outdoor Noise and Heat in Airport Neighbourhoods with Varying Urban Geometries

Gustaf Wuite*[1,2], Zhikai Peng*[1,2], Kyujin Kim[1],Martijn Lugten[1,2], Martin Tenpierik[1]
[1]Delft University of Technology, Delft, the Netherlands
[2]Amsterdam Institute for Advanced Metropolitan Solutions, Amsterdam, the Netherlands

Abstract

This study aims to evaluate the impact of different urban building geometries (six courtyards, two canyons, two slabs) on heat mitigation and aircraft noise attenuation, in order to support an evidence-based retrofit plan for future airport neighborhoods. Using 'Pachyderm + ENVI-met simulations + field measurements', we found that the slanted-roof, low-rise courtyard exhibited optimal acoustic-thermal performance (SPL_{min} = 71.1 dB(A), $\sigma_{UTCI} < 5$ °C), while the mid-rise canyon demonstrated limited performance (SPL_{min} = 93.4 dB(A), $\sigma_{UTCI} > 10$ °C). These findings were observed under averaged boundary conditions of a 140 dB(A) aircraft sound source and a diurnal MRT range of 60 °C on a heatwave day in July 2022.

Nomenclature

Abbr.	Description	Unit
CRY	Courtyard	–
CYN	Canyon	–
FVF	Aircraft view factor	n
MRT	Mean radiant temperature	°C
SD	Sun hour duration	h
Sh	Specific humidity	g/kg
SLB	Slab	–
SPL	Sound pressure level	dB
SVF	Sky view factor	%
Ta	Air temperature	°C
U	Wind speed	m/s
U_{dir}	Wind direction	°
UTCI	Universal thermal climatic index	°C

Introduction

Noise is a main topic in the west and south of Amsterdam in the Netherlands, as the city is wedged in between flight routes from and to Schiphol airport. Placing buildings parallel to these routes can protect a considerable amount of pavement from direct noise exposure, and potentially reduce heat stress if the sun path aligns with the direction of the sound source. A single spatial configuration can have both desired and unfavorable outcomes for noise and heat mitigation. For example, deep street canyons may reduce heat stress but increase noise levels if the facade spacing is too low (Lugten and Kang (2016)). Conversely, open spaces, wide street canyons, and plazas may lead to less reflective sounds but expose pedestrians to more heat and nuisance wind. Some semi-enclosed geometries, like courtyards, exhibit satisfactory acoustic performance (Lugten (2023)) and favorable thermal outcomes (Taleghani et al. (2014), Peng et al. (2023)). This underscores the importance of careful consideration in early-stage urban design to identify optimal spatial strategies to reduce extreme noise and heat stress around the airport neighbourhood. This paper builds upon another contribution (Kim et al. (2023)) to BS 2023, which verified a parametric tool, Pachyderm, using on-site acoustic measurements. Here, we further examine the noise-shielding capabilities of courtyards, street canyons, and slabs that lie beyond the experimental field, as well as investigate their potential for mitigating heat stress.

Materials and methods

We used Pachyderm and ENVI-met software to leverage acoustic-thermal data. The acoustic properties of the concrete slabs and steel walls were pre-tested in Pachyderm, and validated with eight Munisense mics in the field lab. The Pachyderm model settings and accuracy results can be found in Kim et al. (2023). The following section explains the workflow of ENVI-met simulation and spatial analysis for noise and heat mitigation (Figure 1).

In *STEP 1*, a 48-hour heatwave window (18-20 July 2022) was framed to observe the thermal performance of different building types. The KNMI weather data from Schipol airport was synchronised as boundary conditions for the ENVI-met models (Table 1). Although the urban weather generator is recommended for modelling dense-urban contexts with anthropogenic heat effects (Awino (2019)), this weather-morphing technique was not used in this paper because the field lab constructed by shipping containers is located next to the airport.

In *STEP 2*, the thermal properties of the corten steel material were compared (Table 2), following small-scale ENVI-met model validations with four Davis-Kestrel sensors deployed at four locations (V0- outside, V2- shaded, V3- central, and V4- sunlit) in the field lab. Default settings were used for soil and pavement materials to eliminate confounding effects on the differences observed

https://doi.org/10.26868/25222708.2023.1388

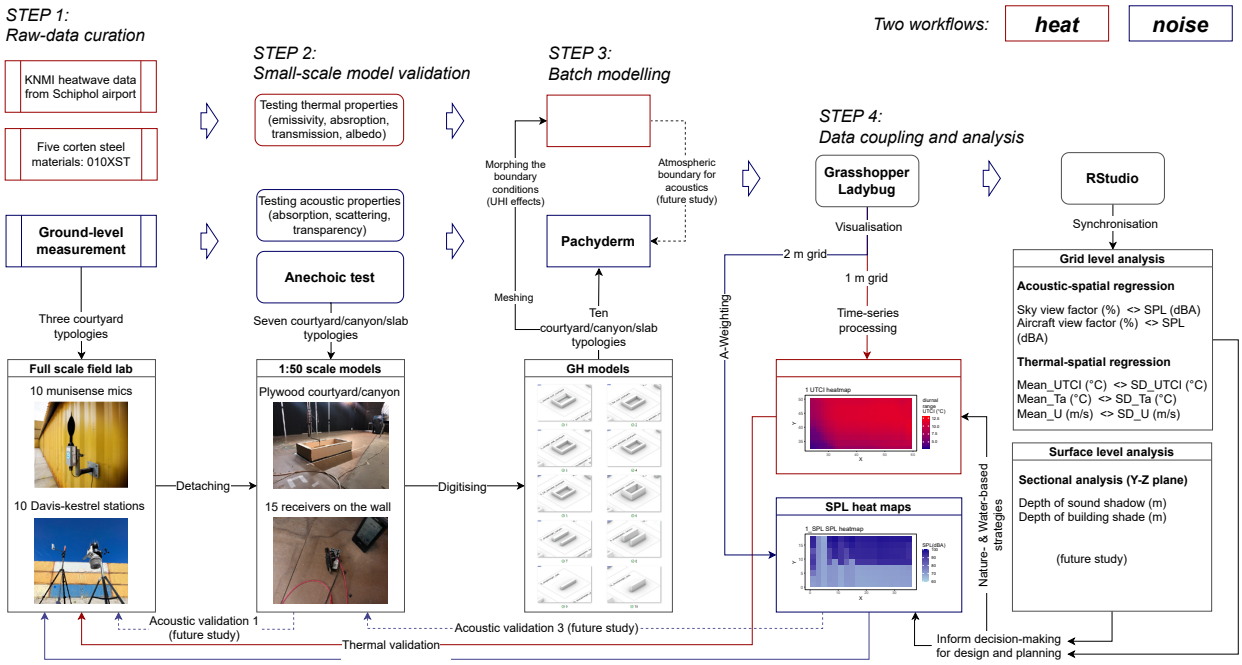

Figure 1: Methodological framework for the integrated noise-heat study (see Appendix I for detailed GH models). Ten GH models, including courtyards, canyons, and slabs, were selected based on their noise-shielding and solar-shading capabilities, as indicated in previous literature. These models incorporate assembly variants such as slanted roofs, elevated walls, and aspect ratios.

between steel materials. Vegetation and water bodies were also excluded from the model as they can potentially complicate the acoustic model as well. The root mean square error (RMSE) was employed to assess the accuracy of the ENVI-met outputs including Ta, Sh, U, and MRT. The globe temperatures (T_g) obtained through Kestrel 5400 heat stress trackers were converted to MRT as the ground-truth observation (Equation 1). According to Walikewitz et al. (2015); Klok et al. (2021), the emissivity of the globe (ε) is 0.95, and its diameter (D) is 150 mm (Kestrel's 1-inch black globe temperature is converted to equivalent 6-inch (150 mm) globe temperature).

$$T_{mrt} = \left((T_g + 273.15)^4 + 1.1 \cdot 10^8 \cdot U^{0.6} \cdot \frac{T_g - T_a}{\varepsilon \cdot D^{0.4}} \right)^{0.25} - 273.15. \quad (1)$$

Table 1: Streamlining of INX and FOX files for 48-hour boundary condition for ENVI-met simulation

Meshing	Mean	Forcing	Mean	Max	Min
X (m)	85	Ta (°C)	29.2	35.0	16.6
Y (m)	86	Sh (g/kg)	7.7	8.2	1.2
Z (m)	40	U (m/s)	2.1	4.1	0.0
Z_{telesc}(m)	9	U_{dir} (°)	164	220	110
Z_{telesc}(%)	9	Cloud (8)	3.7	8.0	0.0

The optimal thermal property for the steel material was selected for batch modelling based on the agreement between simulation and measurement data. As our study focused on building geometry, we did not investigate the acoustic properties but instead used the noise-absorption coefficients from a previous study conducted by Christensen (2002). Future studies could explore how the acoustic and thermal properties of steel materials affect outdoor heat and noise absorption simultaneously, such as density, thickness, and surface texture. So, the thermal validation in our study and the acoustic validation in K et al. (2023) used discrete steel material databases, but share identical acoustic boundary conditions and building typology for validation (Courtyard 1 - 'CRY1', see Figure 5 in Appendix I).

Table 2: Thermal property setting around the courtyard/-canyon/slab: '0100ST' corresponds to the default ENVI-met material database.

Wall material - steel			
ID	Absorption	Reflection	Emissivity
0100ST	0.2	0.8	0.1
0102ST	0.9	0.1	0.9
0103ST	0.7	0.3	0.9
0104ST	0.5	0.5	0.9
0105ST	0.3	0.7	0.9
Soil and pavement			
ID	Material	Reflection	Emissivity
0100LO	Loamy soil	0.8	0.1
0100PL	Concrete light	0.1	0.9

STEP 3 comprises iterative algorithms that enable the automation of batch processing 48-hour ENVI-met sim-

https://doi.org/10.26868/25222708.2023.1388

ulations via a grasshopper plug-in, Dragonfly (the legacy version of *Morpho*). The second 24-hour time-series data were kept for the following spatial analysis. On a DELL workstation, the total simulation of a single building block took approximately 20 hours to complete (12th Gen Intel Core i9-12900K, 3.19 GHz, RAM 64 GB). The simulation time per case for Pachyderm is approximately 10 to 20 minutes, which cannot be automated for batch simulation at this time. The sound pressure level (SPL) results were internalised as data components following each round of Pachyderm simulation.

In *STEP 4*, we combined the thermal and acoustic layers to analyse them at both grid and surface levels. The building-geometrical effects were explored using widely acknowledged spatial variables related to degree of enclosure, such as sky view factor (SVF) and sun hour duration (SD), which can be calculated using the ladybug components. A novel aircraft view factor (FVF) was introduced to measure the unobstructed rays between the grid and sound source. In our study, the maximum FVF value was 9, based on nine sound source positions (P3 to 15) anchored on three flight routes (low, mid, and high, see Figure 5 in Appendix I). To calculate the FVF, simply replace the sun vectors with the noise vectors that are input into the 'sun hour analysis' component in Grasshopper. Notebly, FVF only considers direct sound vectors, excluding reflected ones from opposite building facades. The heat and noise visualisations presented in this paper remain exploratory and descriptive to guide further patch analysis, which may require advanced geo-analytical tools for assessing cool-quiet coverage, locations, and variability (not investigated here).

Results

ENVI-met validation

The study found that the radiation results from ENVI-met are sensitive to the four predefined steel materials with different thermal properties (Figure 2). High-absorptive steel (0102ST) maintained the MRT in the shade (diurnal mean MRT $>$ 30 °C), while high-reflective steel (0105ST) caused an overshoot of the MRT under sunlit circumstances (diurnal mean MRT $>$ 50 °C) due to the reflection of short-wave radiation. The closer the grid was to the steel wall, the greater the influence on MRT. The material's influence on MRT was not as significant at V0, outside of the courtyard. Therefore, we selected the high-absorptive steel (0102ST) for the subsequent batching ENVI-met modelling as it exhibited the lowest RMSEs across four validation positions. The differences in $RMSE_{Ta}$ ($<$ 2 °C), $RMSE_{Rh}$ ($<$ 7 %), and $RMSE_{U}$ ($<$ 0.7 m/s) are not significant between different steel materials. These results align with previous studies that reported over-/underestimations between sun and shade using Kestrel 5400 (Klok et al. (2021)).

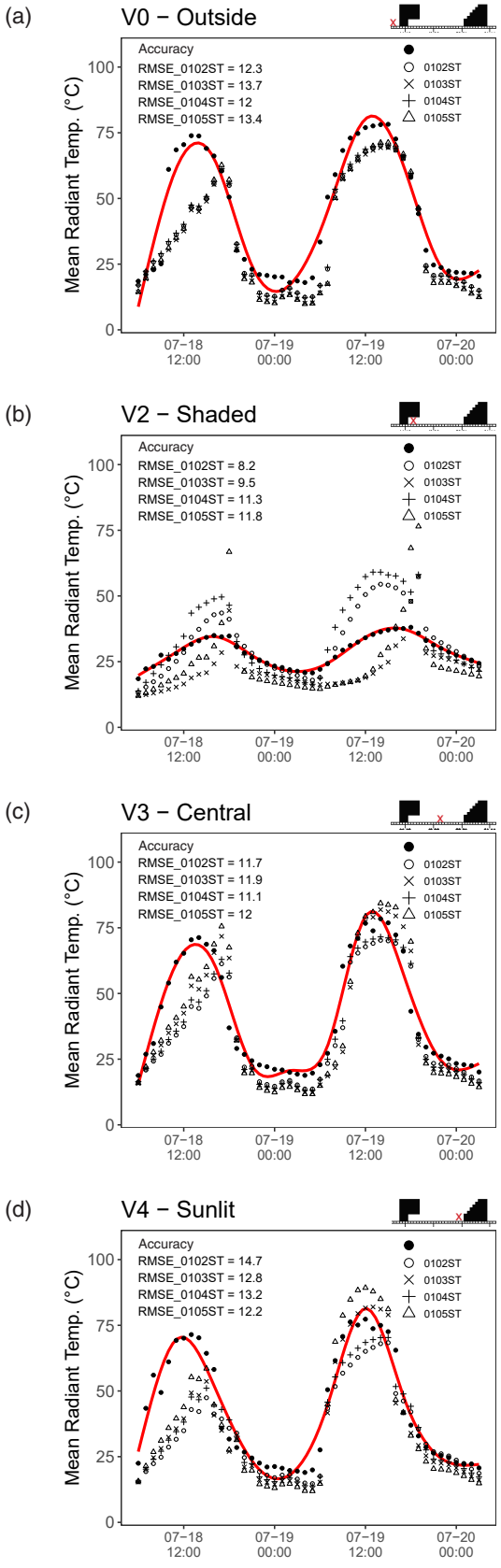

Figure 2: Validation of mean radiant temperature (MRT) for various steel materials at four measurement points (red 'X') in CRY-1 typology. The red lines represent smoothed data derived from Kestrel 5400 data points (ground-truth data in black dots)

https://doi.org/10.26868/25222708.2023.1388

Thermal-spatial regression

Linear regression analyses were performed across all grids in all building types, which have unique time series history of universal thermal climatic index (UTCI) that explains the overall heat stress affected by temperature, humidity, radiation and air flow during day and night (Equation 2).

$$UTCI = f(Ta, Sh, MRT, U_{10m}). \quad (2)$$

Where U_{10m}, the air speed at 10 m height, requires a logarithmic conversion from the ground measurement, which ENVI-met can automate. Although UTCI is not directly available in ENVI-met outputs, it can be calculated in BIO-met using a simplified regression model by Błażejczyk et al. (2013). Next, two statistical metrics are used to explain the intensity and variability of heat stress at each single grid. On the one hand, the diurnal mean UTCI (M_{UTCI}) is used to benchmark the heat stress level between different building typologies. On the other hand, the UTCI swing was introduced by redeveloping the Ta swing indices earlier proposed by Steemers et al. (2004). The UTCI swing was calculated based on the standard deviation of twenty-four UTCI data points (σ_{UTCI}) to evaluate the diurnal thermal range.

The grid-level analysis between diurnal M_{UTCI} and σ_{UTCI} indicates that the sky view factor (SVF) can have a significant effect on heat stress around the courtyards/-canyons/slabs. The higher the visibility of the sky, the more likely a grid will be exposed to heat extremes and experience a larger diurnal thermal range. The results of Ta also align with UTCI, indicating that a higher degree of enclosure (grids with lower SVF, e.g., CRY6 & CYN8 with double heights) can reduce air flow and trap more cold air from the early morning, resulting in a smaller diurnal thermal range (Figure 3-b).

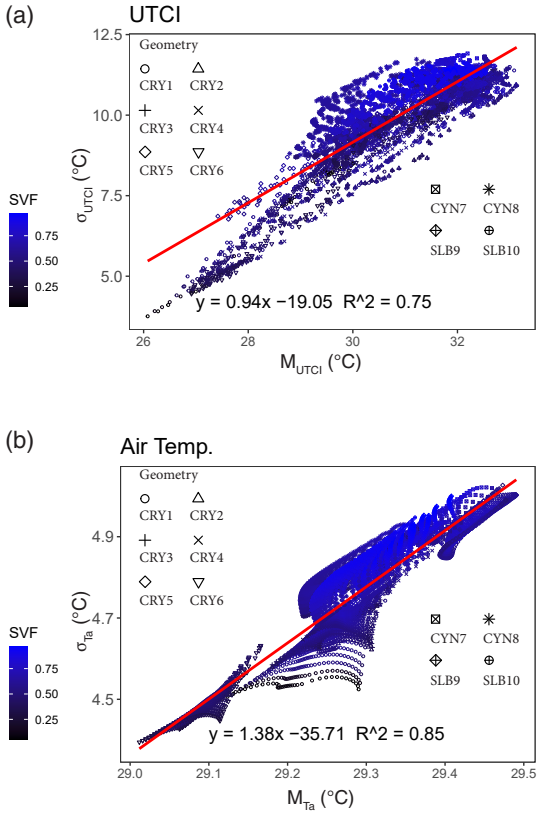

Figure 3: Grid-level analysis of geometric effect based on UTCI (a) and air temperature (b), with color gradients indicating sky exposure of all grids across all building typologies

The thermal regression is corroborated by the surface-level UTCI analysis, which shows that courtyards have a much higher degree of enclosure than canyons and slabs. This is evident from the darker pixels in the bottom-left corner (much lower σ_{UTCI}) among CRY 1 to 6 compared to higher σ_{UTCI} among CYN 7 & 8 and SLB 9 & 10 (see Figure 5-b in Appendix I). The lower diurnal UTCI range can be interpreted as thermal-tempering effects (Peng et al. (2023)), corroborated by many micro-climate and comfort studies in courtyards, especially in warm climates (Rivera-Gómez et al. (2019)).

Acoustic-spatial regression

All grids across all building types have unique A-weighted sound pressure levels (SPLs) from the Pachyderm simulation (Figure 4). The SPL results can be plotted based on nine different aircraft positions, similar to how sun positions can cast different UTCI patterns at different times of the day within the courtyard (See Figure 6 in Appendix II).

The acoustic spatial regressions, while not highly fit, revealed underlying relationships between FVF (non-linear), SVF (linear) and SPLs. Unlike UTCI, the grid with lowest SPL does not correspond to the ones with lowest FVF or SVF. This means that decreasing the

https://doi.org/10.26868/25222708.2023.1388

FVF can only reduce noise to a certain extent, as it also depends on reflected rays from opposite walls (e.g., CRY6 & CYN8 with double heights). Some geometries with higher FVFs and SVFs show significant scattering effects due to slanted roofs (CRY1). There seems to be a lesser reduction of SPL before semi-elevated walls (CRY4), despite Pachyderm not accounting for the diffraction effect under the wall. The noise-shielding effects are especially pronounced in slab typologies with no reflected sound from the opposite side (SLB9 & 10).

The regression fit between SVF and SPL show a much weaker, scattered regression fit (Figure 4-c, d) than that observed between FVF and SPL (Figure 4-a, b), suggesting a weaker impact from the sky than direct sound sources, particularly under high SPL conditions. Despite the challenges, we attempted to establish a partial-regression fit between SVF and low SPL (<80 dBA). The findings suggest that increased sky exposure under low SPL conditions, assumed as situations without direct sound exposure, has the potential to enhance noise attenuation potentials. Note that outdoor sound propagation can be greatly affected by edge refraction and air attenuation. The conclusions of this study and Kim et al. (2023) should be taken with caution since the Grasshopper-Pachyderm algorithms only considered no-wind scenarios and did not account for complicated atmospheric effects, including noise reflections between low clouds and surrounding land cover. Therefore, the lesser impact of SVF only applies to our hypothetical Pachyderm model based on nine aircraft positions anchored on three flight routes.

Another interesting finding is the correlation between FVF and SD. The alignment of the three flight routes and the sun path causes noise and heat sources to accumulate, resulting in higher aircraft sound pressure in sunlit areas. This is especially evident in canyons and slabs compared to courtyards. Our study confirms that static FVF estimation is a valid method for rapidly mapping sound shadow and noise-prone areas caused by aircraft. This simplified estimation can be achieved by replacing sun vectors with sound sources in grasshopper-ladybug, especially for larger urban areas beyond the simulation capacity of Pachyderm. However, this method is unsuitable for hyper-dense areas where noise patterns on the ground level can be dominated by reflected sound rays between closely spaced facades.

Conclusions

Our study on integrated noise and heat in airport neighborhoods has revealed a simulation workflow using Pachyderm-ENVI-met that can assist in decision-making for design and planning. The following are the four main conclusions drawn from our study:

1. The six selected courtyard typologies provide bet-

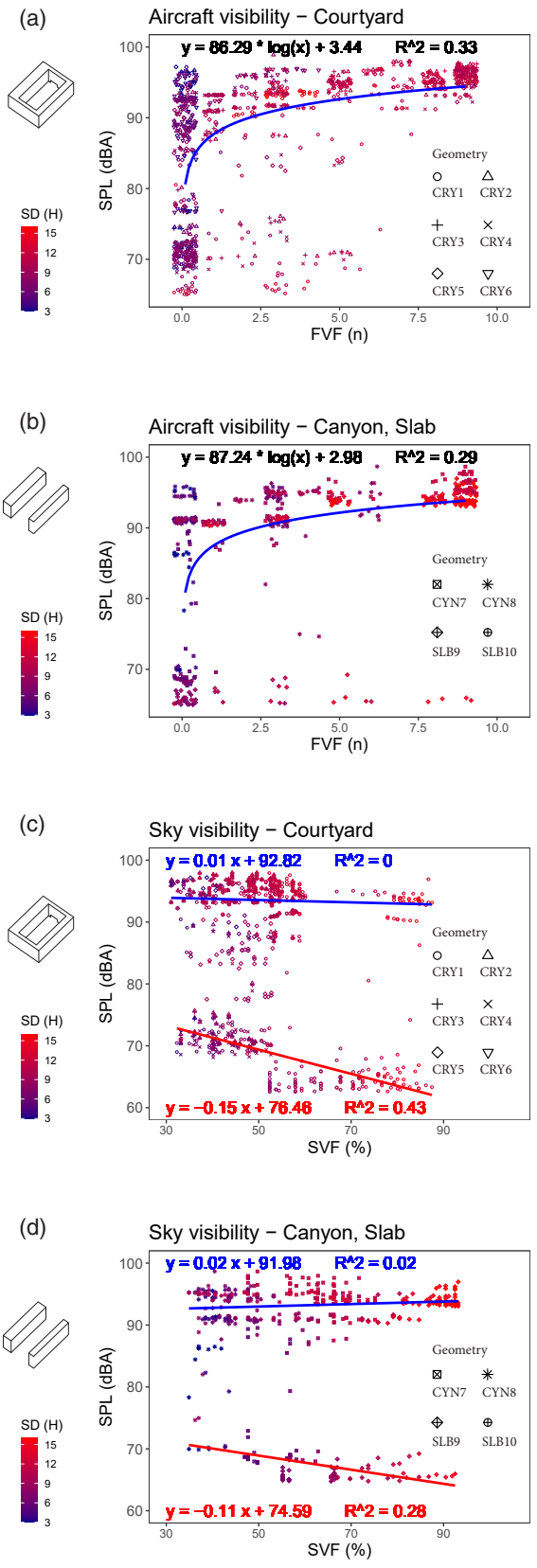

Figure 4: Grid-level analysis of acoustic exposure for courtyards (a) and (c) versus canyons and slabs (b) and (d), with color gradients indicating the diurnal sun duration on 20 July in Amsterdam.

https://doi.org/10.26868/25222708.2023.1388

ter heat-mitigating potentials (more shaded area) but worse noise attenuation (trapping reflected sound rays) than canyons and slabs.
2. Mid-rise buildings reduce heat stress (over 1.5°C reduction in M_{UTCI}) due to mutual shading effects, but compromise noise (over 10 dB(A) increase in M_{SPL}) due to more sound reflections between facades.
3. The slanted roof that scatters direct sound towards the sky is a more effective strategy for noise attenuation than elevating ground floors to reduce the area of sound-facing facades. Therefore, courtyard typologies with slanted roofs remain the optimal choice for achieving good acoustic and thermal performance simultaneously.
4. The study corroborates the acoustic findings of Kim et al. (2023) that the sound source facing direction primarily determines the SPL differences across all building typologies. Pachyderm may underestimate SPLs in shielded areas that receive more bounces in reality.

Last but not least, caution should be taken by architects and landscape designers in applying our conclusions in practise due to the lack of contextualisation of both the simulation models and container field lab in real urban contexts. The further step involves analysing noise and heat in real neighbourhood, taking into account various factors such as building clusters, tree canopies, water bodies, vehicular noise and anthropogenic heat.

Acknowledgment

The two co-first authors (*), G.W. and Z.P. contribute equally to this work. The research is funded by the municipality of Haarlemmermeer, the Dutch ministry for Infrastructure and Water Management, the Dutch ministry for housing and domestic affairs, and the Stichting Leefomgeving Schiphol.

References

Awino, H. R. A. (2019). *Design-integrated Urban Heat Island analysis tool and workflow: Development and application*. Ph. D. thesis, Massachusetts Institute of Technology.

Błażejczyk, K., G. Jendritzky, P. Bröde, D. Fiala, G. Havenith, Y. Epstein, A. Psikuta, and B. Kampmann (2013). An introduction to the universal thermal climate index (utci). *Geographia Polonica 86*(1), 5–10.

Christensen, C. L. (2002). *ODEON room acoustics program version 6.0 usermanual, industrial, auditorium and combined editions*. Technical University of Denmark.

Kim, K., M. Lugten, G. Wuite, Z. Peng, and M. Tenpierik (2023). Assessing the impact of building shape on aircraft noise attenuation: comparison between geometrical acoustics simulation and in-situ measurements. In *Proceedings of Building Simulation 2023: 18th Conference of IBPSA*.

Klok, L., E. Caverzam Barbosa, L. van Zandbrink, and J. Kluck (2021). Application and performance of kestrel sensors for assessing thermal comfort in outdoor built environments. *Proceedings of the EGU General Assembly*.

Lugten, M. (2023). Assessing the influence of street canyon shape on aircraft noise: results from measurements in courtyards near amsterdam schiphol airport. In *INTER-NOISE and NOISE-CON Congress and Conference Proceedings*, Volume 265, pp. 6474–6485. Institute of Noise Control Engineering.

Lugten, M. and J. Kang (2016). An experimental study on the shielding performance of buildings exposed to aircraft noise comparing measurements near front and rear facades. In *INTER-NOISE and NOISE-CON Congress and Conference Proceedings*, Volume 253, pp. 2679–2689. Institute of Noise Control Engineering.

Peng, Z., R. Debnath, R. Bardhan, and K. Steemers (2023). Machine learning-based evaluation of dynamic thermal-tempering performance and thermal diversity for 107 cambridge courtyards. *Sustainable Cities and Society 88*, 104275.

Rivera-Gómez, C., E. Diz-Mellado, C. Galán-Marín, and V. López-Cabeza (2019). Tempering potential-based evaluation of the courtyard microclimate as a combined function of aspect ratio and outdoor temperature. *Sustainable Cities and Society 51*, 101740.

Steemers, K., M. Ramos, and M. Sinou (2004). Urban diversity. In *Environmental Diversity and Architecture*, pp. 85–100. Routledge.

Taleghani, M., M. Tenpierik, A. van den Dobbelsteen, and D. J. Sailor (2014). Heat in courtyards: A validated and calibrated parametric study of heat mitigation strategies for urban courtyards in the netherlands. *Solar Energy 103*, 108–124.

Walikewitz, N., B. Jänicke, M. Langner, F. Meier, and W. Endlicher (2015). The difference between the mean radiant temperature and the air temperature within indoor environments: A case study during summer conditions. *Building and environment 84*, 151–161.

Appendix I

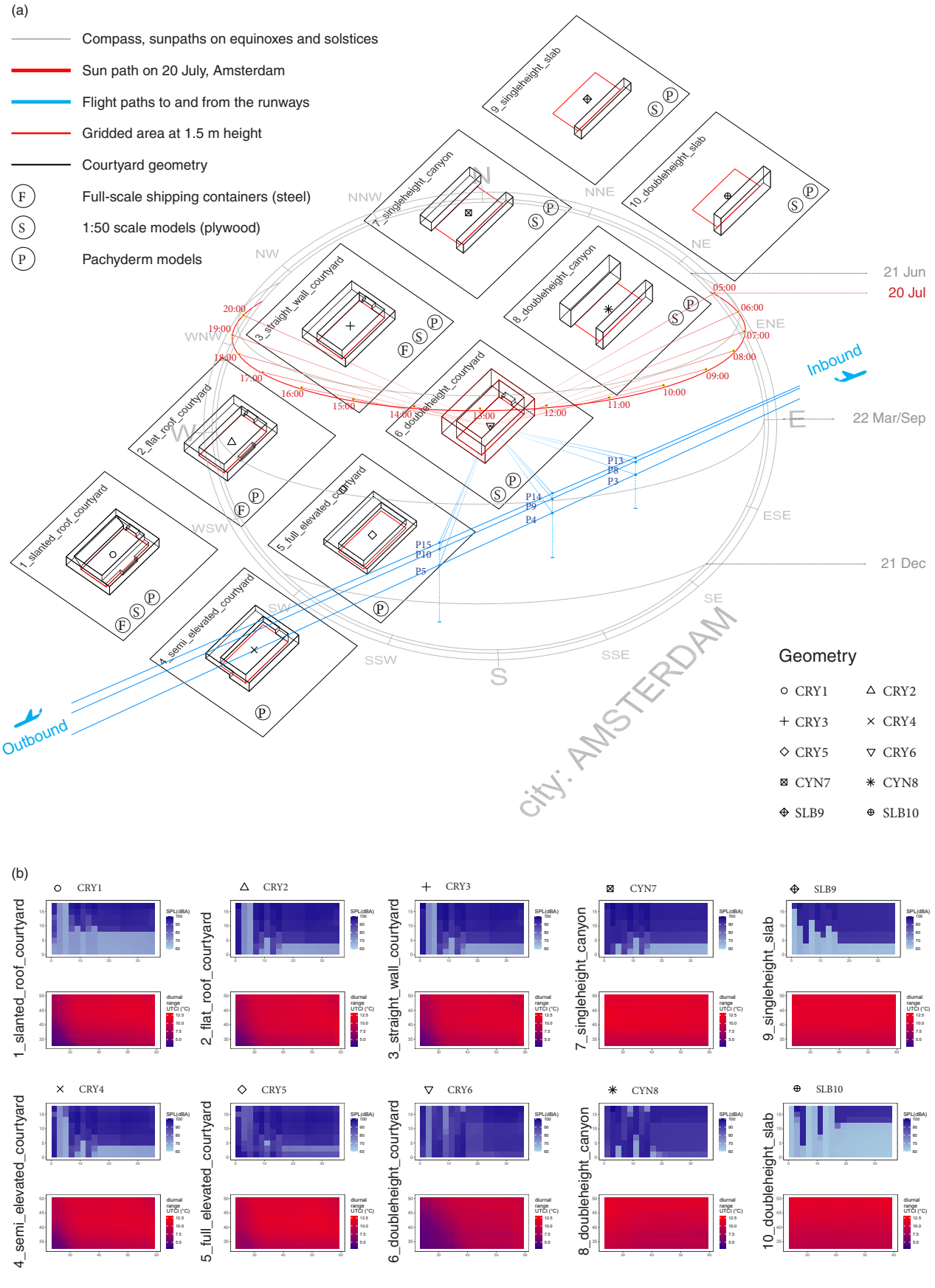

Figure 5: Isometric view from the south showing sun path and flight paths (a), SPL and UTCI maps at a height of 1.5 m (X-Y plane) across ten building typologies, including courtyards, canyons, and slabs (b).

https://doi.org/10.26868/25222708.2023.1388

Appendix II

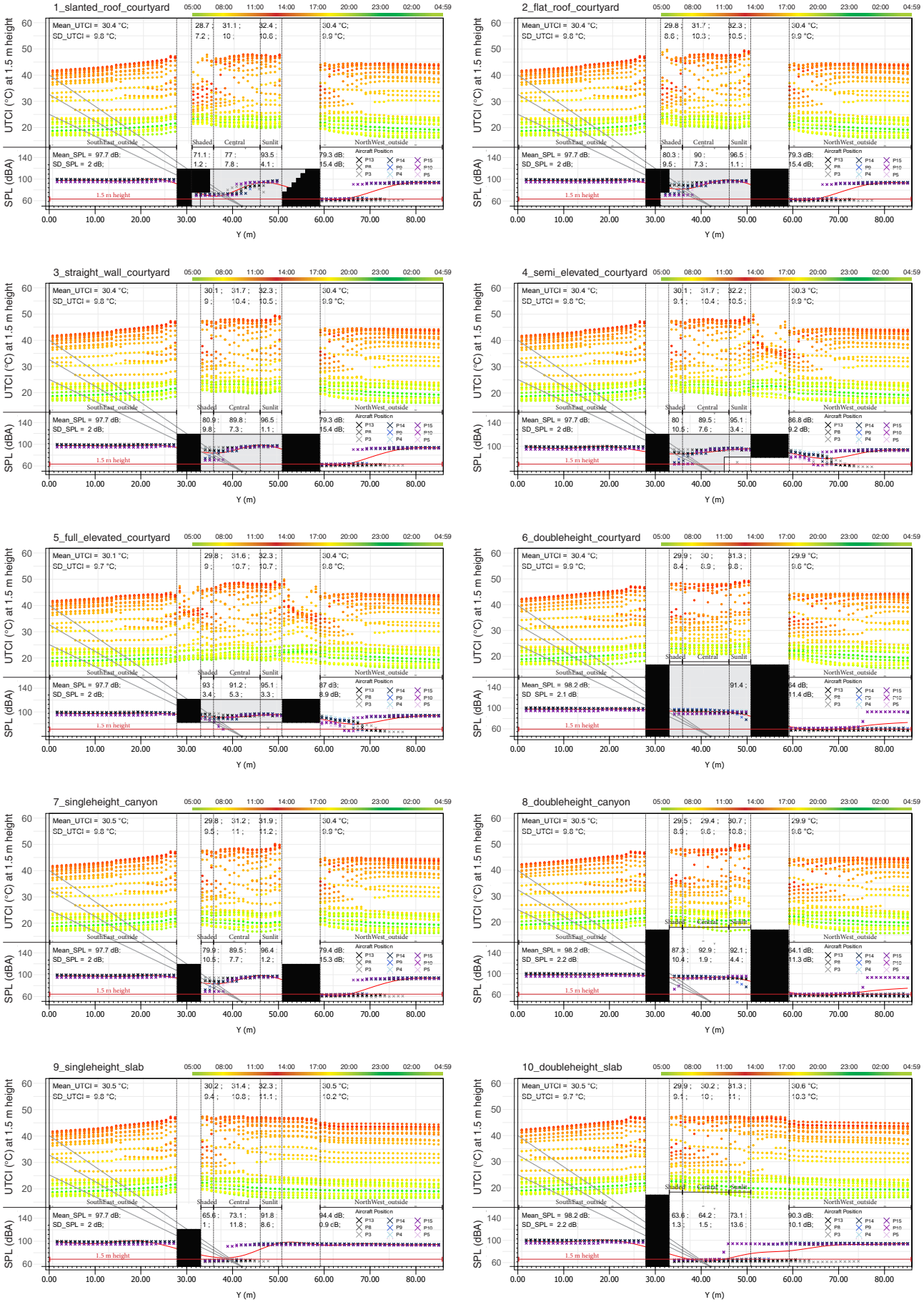

Figure 6: Sectional analysis (Y-Z plane) of UTCI and SPL across ten building typologies, including courtyards, canyons and slabs

https://doi.org/10.26868/25222708.2023.1388